J Appl Electrochem (2009) 39:1487–1495
DOI 10.1007/s10800-009-9828-z

ORIGINAL PAPER

Electrochemical properties of mixed cathode consisting of μm-sized $LiCoO_2$ and nm-sized $Li[Co_{0.1}Ni_{0.15}Li_{0.2}Mn_{0.55}]O_2$ in lithium rechargeable batteries

Kwang Man Kim · Sang Hyo Lee · Sanghyo Kim · Young-Gi Lee

Received: 31 October 2008 / Accepted: 2 February 2009 / Published online: 19 February 2009

Abstract In order to enhance the utilization of active cathode material in lithium rechargeable batteries, physical mixtures of μm-sized $LiCoO_2$ (LCO) and nm-sized $Li[Co_{0.1}Ni_{0.15}Li_{0.2}Mn_{0.55}]O_2$ (LCMNO) were prepared by varying the LCO content, and the physical and electrochemical properties of lithium half-cells utilizing the mixed cathodes were characterized. Our main concern is the packing state between the microparticles and nanoparticles within the electrode, which influences the determination of the electrode density. We found that the electrode composed of 80 wt.% LCO and 20 wt.% LCMNO shows the best performance in capacity retention ratio and high-rate capability, which are comparable to those of LCMNO, due to the superior density in the electrode's packing state over other samples.

Keywords Electrochemical properties · Rechargeable lithium batteries · Mixed cathode material · Electrode packing density

1 Introduction

Using commercially available $LiCoO_2$ (LCO) as the main cathode material in lithium-ion rechargeable batteries provides the desirable properties of both a long plateau at high voltages around 3.7 V and a stable capacity of about 140 mAh g^{-1} for some repeated cycles of charge and discharge. However, this usage has some drawbacks, namely, that LCO contains an expensive cobalt species and exhibits a thermally unstable phase (e.g., thermal runaway may occur at temperatures higher than 220 °C). Studies on cheaper transition-metal oxides have been consequently carried out to replace the expensive LCO, resulting in the high-capacity $Li(Co,Mn,Ni)O_2$-based cathode materials. Of these, $LiCo_{1/3}Mn_{1/3}Ni_{1/3}O_2$ is known to be a very promising cathode material [1–9] because it can provide higher capacity (approximately 200 mAh g^{-1}) and is thermally stable at temperatures above 270 °C. However, $LiCo_{1/3}Mn_{1/3}Ni_{1/3}O_2$ has exhibited some problems when used as the only cathode material in a lithium rechargeable battery due to its low electrical conductivity and low electrode density (or tap density [8, 9]), which results in a decrease in high-rate capability. An alternative way of overcoming such drawbacks is to adopt a mixed cathode material consisting of LCO and $LiCo_{1/3}Mn_{1/3}Ni_{1/3}O_2$ [10–12] with the aim of promoting the two materials' advantages and simultaneously compensating for their disadvantages; for instance, Liu et al. [12] fabricated ICR 18650 cells, adopting a mixture of LCO and $LiCo_{1/3}Mn_{1/3}Ni_{1/3}O_2$ as the cathode and graphite as the anode, which exhibited an increase in high-rate capability at 15 C-rate and improved safety compared with conventional LCO. Noh et al. [11] also showed that the mixed cathode became structurally more stable after heat treatment at 900 °C and then less reactive with surface air so there was no formation of lithium impurities such as Li_2CO_3 and LiOH.

Another benefit obtainable from the mixed cathode of LCO and $Li(Co,Mn,Ni)O_2$ is enhancement in the electrical capacity and energy density by increasing the degree of utilization of the cathode materials, which is possible by increasing the charging voltage to greater than 4.2 V. In

K. M. Kim (✉) · S. H. Lee · Y.-G. Lee
Research Team of Next-Generation Energy Technology, Electronics and Telecommunications Research Institute (ETRI), 161 Gajong, Yusong, Taejon 305-700, South Korea
e-mail: kwang@etri.re.kr

S. Kim
College of Bionanotechnology, Kyungwon University, San 65 Bokjeong, Sujeong, Songnam, Gyeonggi 461-701, South Korea

other words, the crystal lattice deterioration that appeared when the LCO was charged over 4.2 V [13, 14] can be irradiated by the coexistence of the high-voltage cathode $Li(Co,Mn,Ni)O_2$. On the other hand, $Li[Co_{0.1}Ni_{0.15}Li_{0.2}Mn_{0.55}]O_2$ (LCMNO) can be used as a $Li(Co,Mn,Ni)O_2$-based cathode material in the wide voltage range of 2.5–4.5 V, showing the higher capacity of 265 mAh g^{-1} [15]. It can be expected that an increase in capacity would be obtained, as would improvements in cyclability and high-rate capability, if a mixture of LCO and LCMNO were used as a cathode material. In this paper, we prepare cathode electrodes using the mixture composed of varying amounts of LCO, fabricate lithium half-cells using lithium metal foil as anode active material, and finally examine the electrochemical properties of the half-cell in the voltage range 2.5–4.5 V in order to determine the optimal LCO content.

In addition, it should be noted that, in this paper, the cathode mixture consists of powders with different scales of dimension, that is, μm-sized LCO and nm-sized LCMNO. It may be expected that changes will occur in the packing density of the cathode electrode consisting of powders with highly different particle sizes, as a result of fabrication processes such as mixing, milling, coating, and pressing. The altered packing density is then expected to play a significant role in influencing the cathode's electrochemical properties. Thus, we will also consider the packing density as an important factor in the powder mixture with different LCO content throughout this work.

2 Experimental

The LCO powder used was commercially available $LiCoO_2$ from Umicore (KD-10, average diameter 10 μm). The LCMNO powder was obtained via a simple combustion method as described elsewhere [15, 16]. The average diameter of the synthesized LCMNO was measured to be about 250 nm. The powder mixtures were prepared by a simple physical blending of LCO and LCMNO with LCO content increasing from 0, 20, 40, 60, 80, and 100 wt.%, denoted by LCO-0.0, LCO-0.2, LCO-0.4, LCO-0.6, LCO-0.8, and LCO-1.0, respectively. Powder X-ray diffraction measurements were carried out for the mixed samples using an X-ray diffractometer (X'pert Pro, Philips, $\lambda =$ 1.54056 Å) equipped with a Cu target and an accumulative detector. Powder densities were measured for the mixed samples in terms of apparent density using a conventional measuring cylinder, tap density using an autotapper (Quantachrome AT-2, tapping 3,000 times), and true density using a gas pycnometer (AccuPyc 1330 Gas Pycnomer, Micromeritics).

Viscous slurry was obtained by ball-milling the mixed powder (90 wt.%) as an active cathode material, carbon black (Super P, Timcal Graphite & Carbon) (5 wt.%) as a conductive agent, poly(vinylidene fluoride) (KF#1300, Kureha) (5 wt.%) as a polymer binder, and *N*-methyl-2-pyrrolidone (Aldrich) as a solvent at 200 rpm for 2 h to give a homogeneously dispersed state. In the slurry ball-milling, a 40-ml zirconium jar filled with zirconium balls (4 mm diameter, filled about 60 vol.% of the jar) was used, and the ratio of nonvolatile components to liquid solvent was controlled to be about 55 wt.%. A cathode electrode sheet (60–90 μm thick, excluding the aluminum foil as a current collector) was then obtained by coating the slurry on an aluminum foil current collector (15 μm thick) using a doctor-blade apparatus with a gap of 300 μm, then drying in a vacuum oven at 90 °C for 1 h to evaporate the solvent component, and finally pressing using a double-roll press with a line pressure of 1,000 kg_f cm^{-1} at room temperature. The surface morphologies of the electrodes were observed with a field-emission scanning electron microscope (FE-SEM, Jeol JSM-7000F).

A lithium half-cell was then fabricated by (i) superimposing the [cathode (1.5 cm × 1.5 cm)‖polyethylene separator (2.5 cm × 2.5 cm)‖lithium metal foil (2 cm × 2 cm)] in sequence, (ii) packaging in an aluminum bag after the injection of an electrolyte solution (1 M $LiPF_6$ in an equal-weight mixture of ethylene carbonate and dimethyl carbonate), and (iii) vacuum-sealing and aging the mixture for at least 6 h. A nickel mesh (2 cm × 2 cm) was used as the current collector for the lithium metal anode. All the fabrication steps were carried out in a dry room in which a nearly moisture-free condition was maintained with a dew point of less than −40 °C. In order to examine the redox characteristics of the electrode adopting the mixed active materials, cyclic voltammetry (CV) tests were carried out using a potentiostat (Solartron 1480 Multistat equipped with Solartron 1400/1470E). The CV tests featured similar conditions to the charge–discharge test: a scan rate of 0.1 mV s^{-1} in the range of 2.0–4.8 V (versus Li/Li^+) for the first cycle and 0.2 mV s^{-1} in 2.5–4.5 V (versus Li/Li^+) for the second to sixth cycles. The lithium half-cells were also subjected to galvanostatic cycling using a charge–discharge cycler (Toscat 3000, Toyo Systems) and a constant current of 0.1 C-rate in the range of 2.0–4.8 V for the 1st cycle and 0.2 C-rate in the range of 2.5–4.5 V for the 2nd to 51st cycles. The voltage was raised to 4.8 V in the first cycle to ensure high capacity with a long plateau over 4.5 V [15, 16], whereas the voltage was limited to 4.5 V from the second cycle onward due to concerns about electrochemical stability and/or safety. That is, it could be expected that the LCMNO prevented the deterioration of LCO when charging over 4.2 V in the mixed state, but the limitation of charging to 4.5 V (except for the first cycle) was for the electrochemical stability and/or safety of the other substances such as the polymer binder and electrolyte components. In addition, we observed the surface states of the electrodes and

separators when disassembling the lithium half-cells after the 51st cycle. A rate-capability test was also performed in the potential range of 2.0–4.8 V at the rate of 0.1 C-rate (1st cycle), 2.5–4.5 V at 0.2 (2nd to 6th cycles), 0.3 (7th to 11th cycles), 0.5 (12th to 16th cycles), 0.7 (17th to 21st cycles), 1.0 (22nd to 26th cycles), 2.0 (27th to 31st cycles), and 3.0 C-rate (32nd to 36th cycles) in sequence.

3 Results and discussion

Figure 1 shows X-ray diffraction patterns of the mixed powders of LCO and LCMNO. A comparison of the peaks of pure LCO (i.e., LCO-1.0) and pure LCMNO (i.e., LCO-0.0) shows that most peaks corresponding to each plane of LCMNO shift slightly in the direction of the low Bragg angle. The mixed powders show two neighboring peaks for the same plane of lattice crystal, one corresponding to LCO and the other to LCMNO, because of the simple physical blending. For instance, sample LCO-0.6 exhibits two peaks at $2\theta = 18.5°$ and 19.0°, which correspond to the (003) plane of LCMNO and LCO, respectively. In addition, the peaks of (006) and (009) (indicated by * in the figure) in LCO did not appear in LCMNO, but appeared with weak intensities in the mixed samples. This suggests that the physical blending of the powders is well established.

On the other hand, the electrode density strongly depends on the packing state even when the two types of powders with different particle sizes have been physically blended, because the average size difference between the two materials is 40 times. That is, the average size of the LCO particles is 10 μm while the average size of the LCMNO particles is 250 nm. In particular, different packing states may occur when the LCO content differs

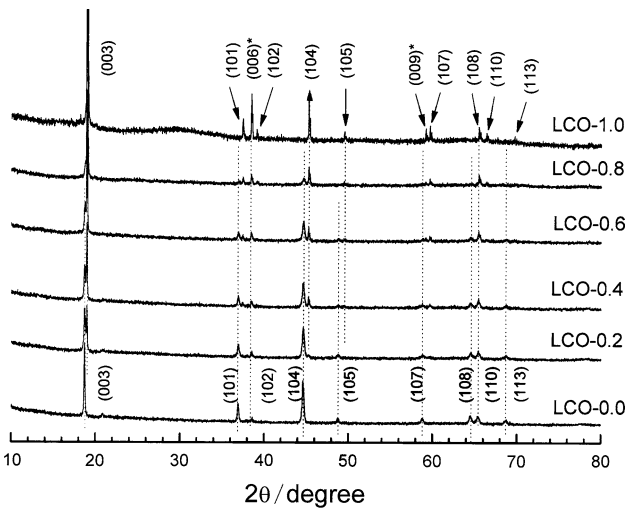

Fig. 1 X-ray diffraction patterns of mixed powders of LCO and LCMNO

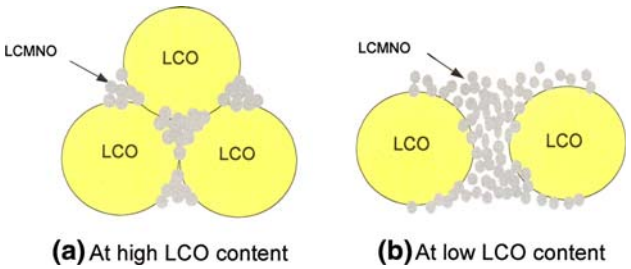

Fig. 2 Schematic diagram of packing states of the mixed powders with **a** a high LCO content and **b** a low LCO content

from the LCMNO content, as shown schematically in Fig. 2. When the content of LCO particles is higher than that of LCMNO, small LCMNO particles may occupy the cavities between the larger LCO particles and the mixture then exhibits a close packing state. On the other hand, when the LCO content is lower than the LCMNO content, the number of small LCMNO particles may be insufficient to occupy the cavities between the large LCO particles, which results in a loose packing state. The density of the electrode, consisting of a mixture of LCO and LCMNO powders, is thus closely related to the packing density of the powders and their processing conditions (such as coating, drying, and pressing), as the electrode contains the active material (the powder mixture) as well as other substances such as the conductive agent powder and the polymer binder. The various densities of the mixed powder and the electrode densities are summarized in Table 1. The porosity of the electrode as a factor that ensures good ionic transport is temporarily excluded in this study due to the complexity of considering an additional issue.

The apparent density is based on the volume that includes both the inner pores of the particles and the cavities between the particles when packed naturally under gravitational force. In contrast, the true density is based on the volume that excludes all the inner pores and the cavities. The tap density may be regarded as the closest packing state of the powder obtained by tapping (3,000 times in the present work) and is strongly related to the electrode density. The electrode density, calculated from the weight/volume of the electrode sheet (2 cm × 2 cm, excluding the aluminum foil current collector), includes small contributions from the conductive agent and the polymer binder. It should be noted that the electrode sheet is produced via the fabrication processes, especially by double-roll pressing to increase its packing density. As shown in Table 1, the electrodes that contain the powder mixtures exhibit slightly lower electrode densities than their tap densities, except for the LCO-0.0 and LCO-0.8 samples. If we consider the tap density as that with the closest packing, the lower electrode density indicates the possibility of further packing. However, the LCMNO (i.e., LCO-0.0) shows a slightly higher

Table 1 Summary of various powder densities and the electrode density

Sample	Apparent density (g cm^{-3})	Electrode density[a] (g cm^{-3})	Tap density (g cm^{-3})	True density (g cm^{-3})
LCO-0.0	0.97	1.74	1.59	4.07
LCO-0.2	1.09	1.14	1.73	4.29
LCO-0.4	1.23	1.22	1.85	4.54
LCO-0.6	1.27	1.71	1.99	4.74
LCO-0.8	1.43	2.18	2.20	5.08
LCO-1.0	1.94	2.38	2.66	5.29

[a] Including conductive agent and polymer binder, excluding the current collector (Al foil)

electrode density (1.74 g cm^{-3}) than the tap density (1.59 g cm^{-3}), which indicates that overpacking of the 250-nm-sized LCMNO particles has occurred during the slurry ball-milling and double-roll pressing processes. In the electrodes with low LCO content, there is increased probability of voids occurring between many 250-nm-sized LCMNO particles and a few of the 10-μm-sized LCO particles, indicating that closest packing has not been achieved. In such cases, a highly porous surface is produced. An increase of the packing state above the mean law for mixtures of μm-sized and nm-sized particles can be easily observed [17]. However, the electrodes with high LCMNO content show lower packing densities than the mean packing state between those containing LCO and LCMNO alone. This could have occurred due to insufficient pressing, as pressing is needed to compensate for the increased probability of the appearance of voids (Fig. 8). Aside from providing surface morphologies of the electrode, cross-sectional images will be helpful in describing such situations in detail (but are not shown in this paper).

In contrast, LCO-0.8 exhibits an electrode density (2.18 g cm^{-3}) similar to the tap density (2.20 g cm^{-3}), which denotes that the closest packing state is nearly achieved by the mixing, as in the case of Fig. 2a. Moreover, these packing states can be confirmed by the surface morphologies of the electrodes, as shown in Fig. 3. For instance, the surface image of the LCO-0.8 sample shows the homogeneous distribution of LCMNO nanoparticles in the voids among the large LCO microparticles, which gives an extremely effective packing state. It may be expected that the effective packing state is beneficial to obtain a superior electrochemical performance by increasing the utilization of active materials.

As shown in Fig. 4, the cyclic voltammogram in the first cycle is obtained in the potential range of 2.0–4.8 V (versus Li/Li^+) at a scan rate of 0.1 mV s^{-1}, similar to the conditions of the first cycle of the charge–discharge test. For the sample of LCMNO (Fig. 4a), the single oxidation peak at about 4.1 V in the first cycle corresponds to $Co^{3+/4+}$ [18]

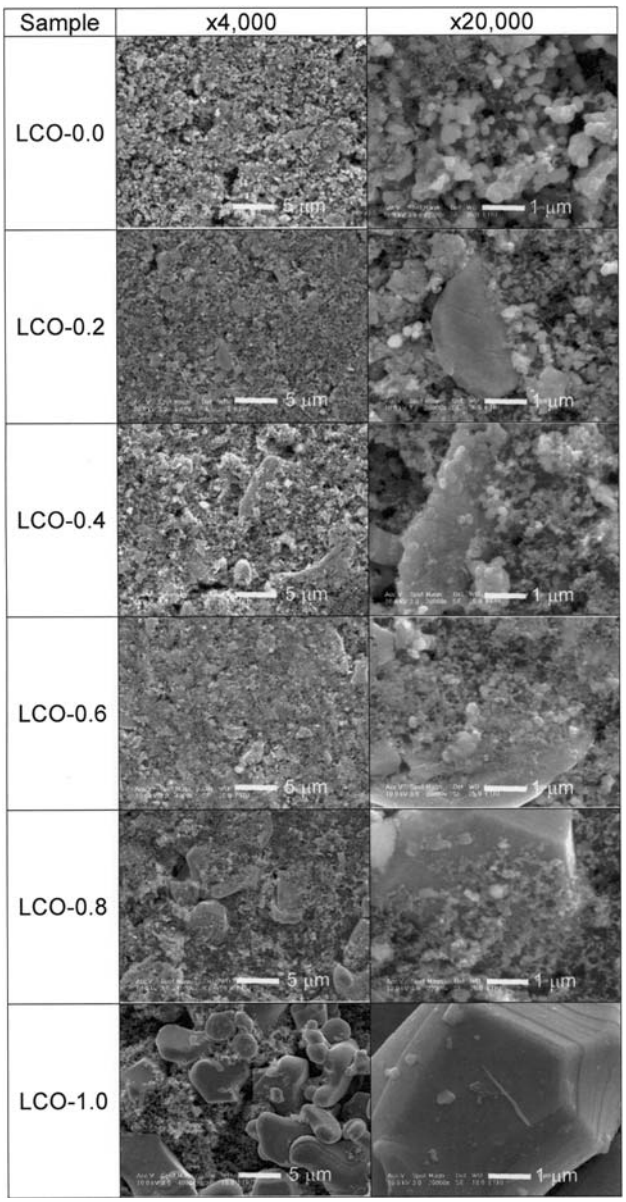

Fig. 3 Scanning electron micrographs of electrode surfaces with magnification ratios of 4,000× and 20,000×

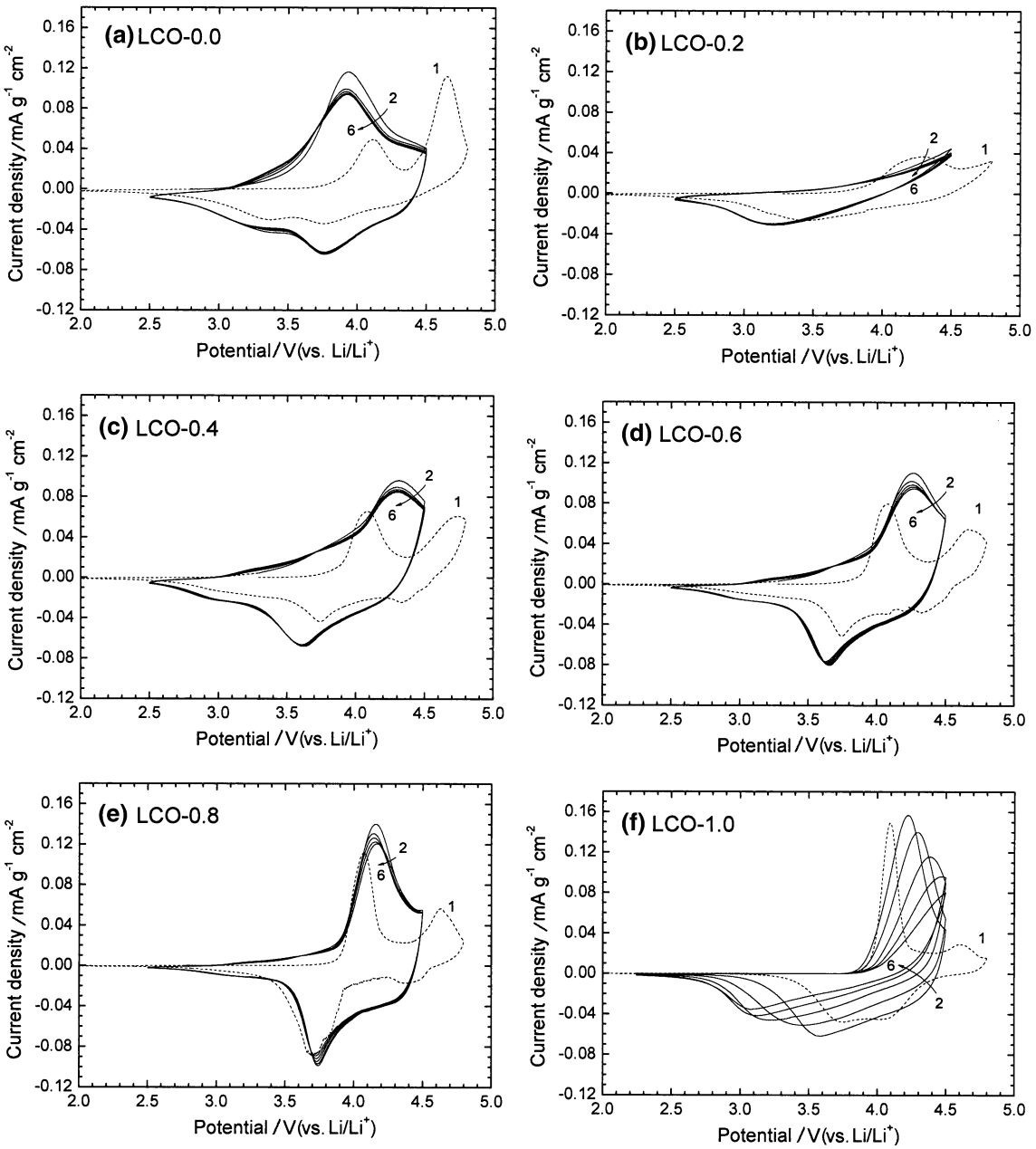

Fig. 4 Cyclic voltammograms of the lithium half-cells adopting the mixed powders as the cathode active materials. The first cycle was operated at 0.1 mV s^{-1} between 2.0 and 4.8 V (versus Li/Li^+) whereas the other cycles were operated at 0.2 mV s^{-1} between 2.5 and 4.5 V (versus Li/Li^+). The numbers in the figure denote the cycle numbers

and, more precisely, to the superposition of $Ni^{2+/3+}$ and $Co^{3+/4+}$ oxidation peaks caused by Co^{3+} acting as a catalytic center [15]. According to a recent report [19], Ni^{2+} is directly oxidized to Ni^{4+}, rather than to Ni^{3+}. The high-intensity peak at about 4.6 V, which is usually observed in the layered structure of manganese oxide, may be due to a loss of oxygen with manganese species remaining in the Mn^{4+} state [19]. In practice, the higher capacity of the LCMNO may be achieved from the fact that the intercalation–deintercalation of Li^+ can easily occur deep within the layered-structure manganese oxide matrix at the oxidation potential of Mn^{4+}. However, the contribution of the manganese species is limited because the potential is restricted to the range of 2.5–4.5 V after the second cycle, while the cyclic voltammogram shows a very symmetric shape with a high reversibility. The main oxidation peak at 3.9 V after the second cycle corresponds to the cobalt species, which is shifted from the peak at 4.1 V at the first cycle.

The reduction peak that appears at 3.75 V can be regarded as being due to the reduction of Ni^{4+} to Ni^{2+}, and the small peak below 3.5 V to the reduction of manganese species.

Furthermore, the LCO sample (Fig. 4f) shows that the oxidation peaks appear only at potentials higher than 4.0 V. The peak at 4.1 V in the first cycle, which corresponds to the cobalt species, shifts to the higher potential range with diminishing intensity as the cycle number increases. This is due to the partial structural deterioration by the overoxidation of the cobalt species [13, 14] or side-reactions between the LCO surface species and $LiPF_6$-based electrolytes [20] during oxidation up to 4.8 V in the first cycle. The structural deterioration may then be accumulated by the repeated oxidation–reduction in the potential range of 2.5–4.5 V, leading to poor cycle performance. Correspondingly, it is a matter of course that the reduction peak at 3.75 in the first cycle shifts to lower potential range with diminishing intensity as the cycle number increases.

As a case of low LCO content, the LCO-0.2 sample (Fig. 4b) shows a weak oxidation peak at 4.25 V and the corresponding broad reduction peak at 3.4 V in the first cycle. After the second cycle, easily reversible redox responses with weak intensity appear, except for a broad reduction peak at 3.2 V. The electrode state in this case is an insufficient packing of nm-sized LCMNO particles distributed dominantly with small amounts of μm-sized LCO particles (Fig. 2b). The insufficient packing can be associated with a high deviation between the electrode density and tap density (Table 1), which can lead to low electrical conductivity and poor utilization of the active materials. Thus, it not only inhibits the oxidation of LCMNO's cobalt species at 4.25 V, but also decreases the electrochemical activity after the structural deterioration of LCO that occurs from charging to 4.8 V in the first cycle. However, it is fortunate that small amount of surviving active sites exhibit a very reversible redox response in the potential range of 2.5–4.5 V after the second cycle.

As the LCO content increases, the CV pattern starts to appear as an intermediate form between the LCO and LCMNO responses. This indicates that each powder participates in the electrochemical redox reaction and plays its own role sufficiently. Common features found in Fig. 4c–e are as follows: (i) the oxidation peak of cobalt species appears at 4.1 V and its corresponding reduction peak at 3.75 V in the first cycle, (ii) such peaks shift to 4.1–4.3 V and 3.6–3.7 V, respectively, with good reversibility between 2.5 and 4.5 V after the second cycle. The reversibility may be achieved by the efficient packing state of the LCO and LCMNO, in which each powder contributes its own potential to the electrochemical redox reaction. In addition, the symmetric shape of the CV response becomes enhanced with increase in LCO content. In particular, the LCO-0.8 sample shows highly reversible, higher current responses in the oxidation at 4.15 V and the corresponding reduction at 3.7 V, which is due to an efficient packing state of the electrode consisting of 80 wt.% LCO and 20 wt.% LCMNO.

Initial charge–discharge profiles are shown in Fig. 5a for the first cycle operated between 2.0 and 4.8 V at 0.1 C-rate. As in the results of Hong et al. [15], LCMNO is able to ensure the higher capacity with a long plateau at 4.5 V in the charging process and thus shows an initial discharge capacity higher than 259 mAh g^{-1} in the potential range of 2.0–4.8 V. On the other hand, the LCO barely shows any plateau in the charging process to 4.8 V, but exhibits a long plateau at about 3.9 V and an abrupt voltage drop at about 3.7 V, with a discharge capacity of 230 mAh g^{-1} in the discharging process. Contrary to the conventional plateau of LCO at 3.7 V in the charge–discharge between 3.0 and 4.2 V, the rise of plateau voltage is considered to be due to

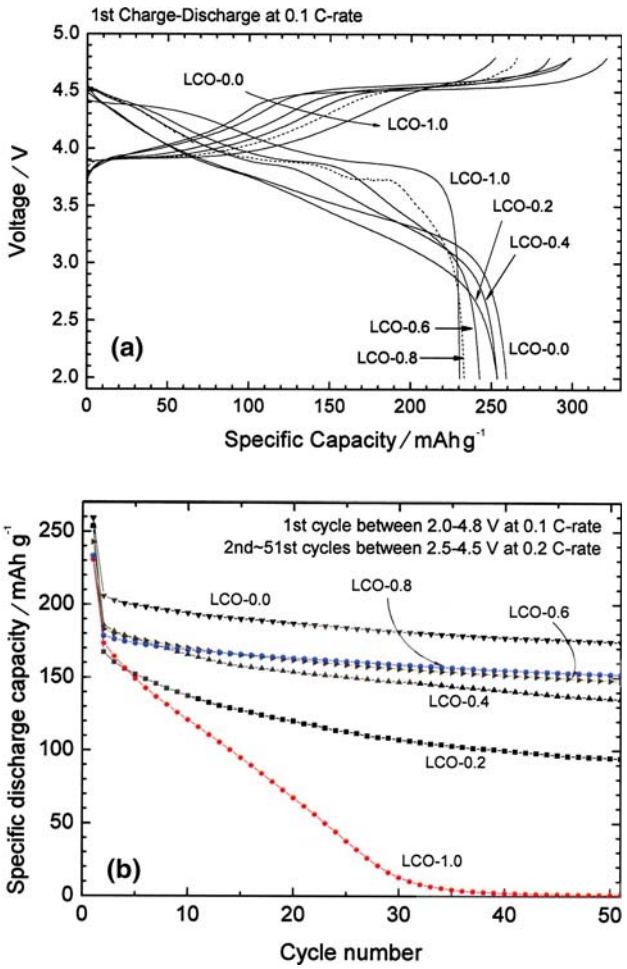

Fig. 5 **a** Charge–discharge profiles for the first cycle and **b** cycle performance of the lithium half-cells adopting the mixed powders as the cathode active materials. The first cycle was operated at 0.1 C-rate between 2.0 and 4.8 V (versus Li/Li^+) whereas the other cycles were operated at 0.2 C-rate between 2.5 and 4.5 V (versus Li/Li^+)

the charging to 4.8 V, which may involve structural deterioration of LCO [13, 14] or side-reactions with electrolytes [20]. Compared with approximately 140 mAh g^{-1} for LCO from the conventional charge–discharge condition between 3.0 and 4.2 V, the initial discharge capacity of 230 mAh g^{-1} is a much higher value, but this decreases abruptly with the accumulation of structural instability over repeated charge and discharge (Fig. 5b). The addition of a small amount of nm-sized LCMNO to the μm-sized LCO can be expected to aid in avoiding such severe capacity fade because the high-voltage property of LCMNO may help in resisting the structural collapse of LCO. As shown in Fig. 5a, the mixed cathode samples generally show intermediate forms between LCO and LCMNO, but the LCO-0.2 sample suffers from inefficient utilization of electrochemical active sites due to comparatively coarse packing states that results in poor initial electronic contact and rapid contact loss during cycling, and thus in a lower discharge capacity than expected (cf. Table 2). Furthermore, the specific discharge capacity from the second cycle operated at 0.2 C-rate shows a lower value than in the first cycle at 0.1 C-rate. Except for in the LCO-0.2 sample, the discharge capacity in the second cycle decreases with the increase in the LCO content (Table 2), due to efficient contributions of LCO and LCMNO in the electrochemical reaction. For the LCO-0.2 sample, the largest decrease ($253.8 - 167.2 = 86.6$ mAh g^{-1}) in the discharge capacity between the first and second cycles can be regarded as being due to insufficient contact between active material particles, as discussed above.

As shown in Fig. 5b and Table 2, the capacity retention ratio (based on the discharge capacity in the second cycle) shows that the LCO-1.0 suffers an abrupt decrease in discharge capacity. This was caused by the accumulation of cobalt species deposited on the separator, which originated from the structural deteriorations of LCO over 4.2 V during the repeated charge–discharge (see the image in Fig. 6b). In Fig. 6, the cathode side faces up for the separator. The cycle performance can be improved by the addition of small amounts of high-voltage-resistive LCMNO powders; for instance, the LCO-0.8 sample exhibits a superior capacity retention ratio (85.2% after 51st cycle) to the other samples and also shows a comparable capacity retention ratio to that of LCMNO itself (84.7% after 51st cycle). This can be evidenced by the images of disassembled electrodes and separators after cycling the lithium half-cell 51 times, as shown in Fig. 6a. That is, comparatively clean surfaces of the polyethylene separator and cathode appear without any deposition of lithium and/or other metal species (i.e., Co, Mn or Ni), which verifies the reversible deposition-stripping of lithium cations and/or lack of dissolution of other metal species during the repeated charge–discharge. Only a small amount of lithium dendrite is formed between lithium metal anode and separator.

Figure 7 shows the rate-capability results obtained after varying the range from 0.2 to 3.0 C-rate for lithium half-cells adopting the mixed cathode samples. At low current rates, most samples, except for the LCO, exhibit discharge capacities comparable to that of LCMNO. As the current rate increases up to 0.7 C-rate, the LCO-0.8 and LCMNO samples maintain their discharge capacities. However, only the LCMNO can deliver a higher discharge capacity at current rates above 1.0 C-rate. That is, the LCO-0.8 sample has a decent packing structure that promotes the efficient transport of lithium cations; thus, it shows a higher rate capability during cycling between 2.5 and 4.5 V. At current rates above 1.0 C-rate, however, the LCO-0.8 sample no longer behaves as an active material that is more useful than the high-voltage-resistive LCMNO.

Table 2 Discharge capacities and capacity retention ratios

Sample	Discharge capacity (mAh g^{-1})		Capacity retention ratio[c] (%)	
	At 1st cycle[a]	At 2nd cycle[b]	At 21st cycle	At 51st cycle
LCO-0.0	259.4	205.8	90.3	84.7
LCO-0.2	253.8	167.2	70.2	56.5
LCO-0.4	253.7	185.7	82.0	72.8
LCO-0.6	242.8	182.9	87.7	80.8
LCO-0.8	233.2	178.3	91.0	85.2
LCO-1.0	230.5	173.3	32.2	0.4

[a] Obtained at 1st cycle operated between 2.0 and 4.8 V at 0.1 C-rate

[b] Obtained at 2nd cycle operated between 2.5 and 4.5 V at 0.2 C-rate

[c] Capacity retention ratio (%) = (discharge capacity at the cycle/discharge capacity at 2nd cycle) × 100

4 Conclusions

We have reported the electrochemical characteristics of a mixed cathode consisting of μm-sized LCO and nm-sized LCMNO powders in an effort to enhance the utilization of active cathode materials in lithium rechargeable batteries. In the fabrication of lithium half-cells that adopt the mixed cathode, the electrode density is the primary consideration to provide a superior packing state, associated with the tap density of the mixed powder. A summarized figure for the powder and electrode densities can be suggested (Fig. 8), which is associated with the electrode performances obtainable when adopting the mixed cathodes. In the present study, the electrode consisting of 80 wt.% LCO and 20 wt.% LCMNO showed the best performance in terms of capacity retention ratio and high-rate capability,

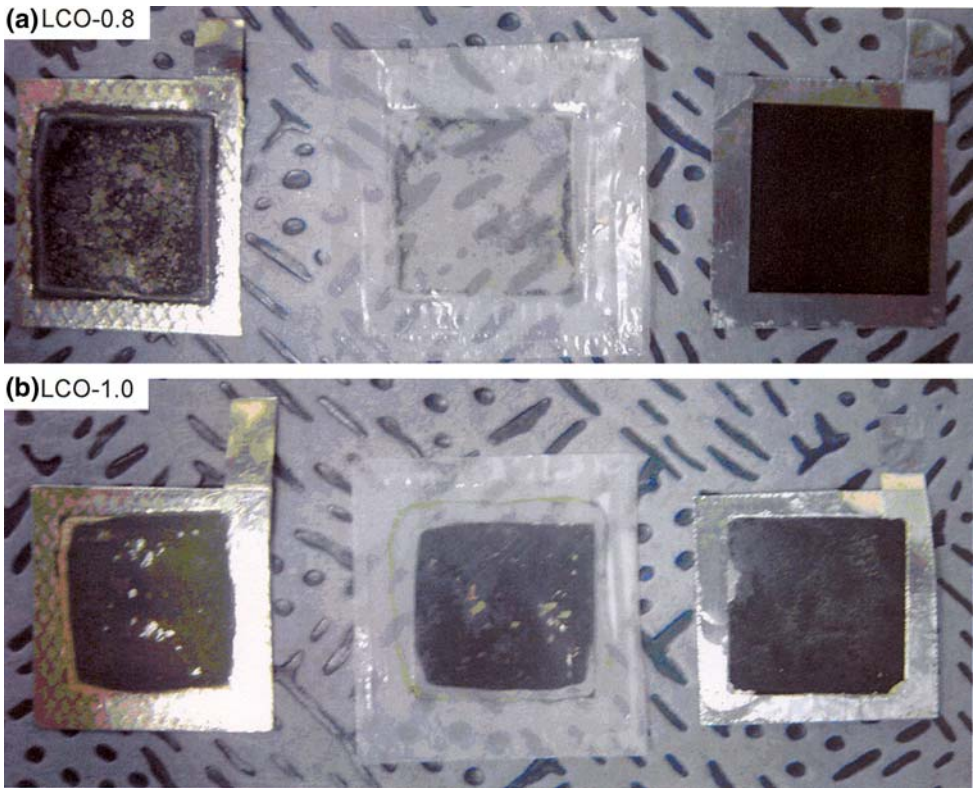

Fig. 6 Disintegration images of the lithium half-cells after the 51st cycle, adopting **a** LCO-0.8 or **b** LCO-1.0 samples as the cathode active materials. Lithium metal anode, separator, and cathode are seen from left to right. The cathode side is up for the separator

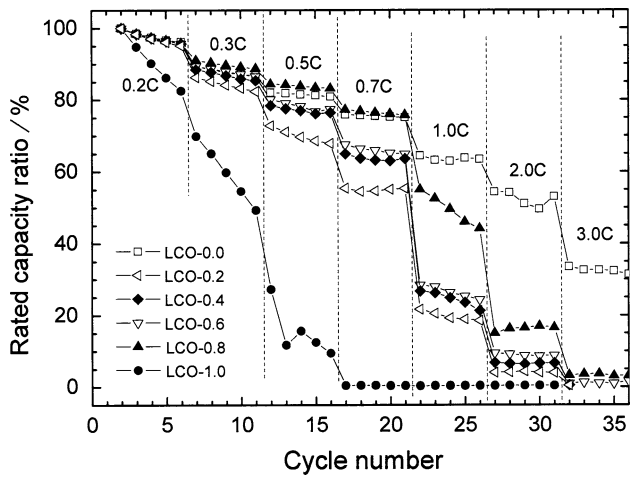

Fig. 7 Rate capabilities of lithium half-cells using the mixed powders as the cathode active materials. The rated capacity ratio (%) is determined by considering the discharge capacity in the second cycle as 100%

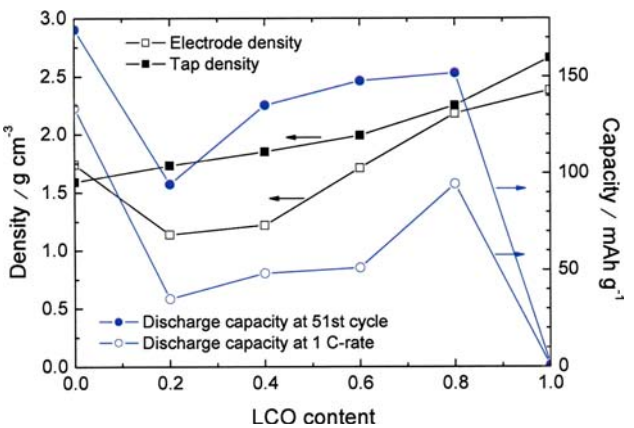

Fig. 8 Summary of some important densities and discharge capacities in this work

being comparable to those of LCMNO, due to the superior compactness in the packing state of the electrode compared with other samples. Electrodes with higher packing states show better electronic contact and better maintenance during cycling. Finally, even small additions of LCMNO preserve the cycling stability of LCO and suppress the decomposition of LCO.

References

1. Yabuuchi N, Ohzuku T (2003) J Power Sources 119–121:171
2. Koyama Y, Tanaka I, Adachi H, Makimura Y, Ohzuku T (2003) J Power Sources 119–121:644
3. Shaju KM, Rao GVS, Chowdari BVR (2002) Electrochim Acta 48:145
4. Shaju KM, Rao GVS, Chowdari BVR (2004) J Electrochem Soc 151:A1324
5. Kim MG, Shin HJ, Kim J-H, Park S-H, Sun Y-K (2005) J Electrochem Soc 152:A1320

6. Zhang L, Wang X, Muta T, Li D, Noguchi H, Yoshio M, Ma R, Takada K, Sasaki T (2006) J Power Sources 162:629
7. Smart MC, Whitacre JF, Ratnakumar BV, Amine K (2007) J Power Sources 168:501
8. Zhang S (2007) Electrochim Acta 52:7337
9. Chang Z, Chen Z, Wu F, Tang H, Zhu Z, Yuan XZ, Wang H (2008) Electrochim Acta 53:5927
10. Kim H-S, Kim S-I, Kim W-S (2006) Electrochim Acta 52:1457
11. Noh M, Lee Y, Cho J (2006) J Electrochem Soc 153:A935
12. Liu X, Zhu G, Yang K, Wang J (2007) J Power Sources 174:1126
13. Ohzuku T, Ueda A (1994) J Electrochem Soc 142:2972
14. Amatucci G, Tarascon JM, Klein LC (1996) Solid State Ionics 83:167
15. Hong Y-S, Park YJ, Ryu KS, Chang SH, Shin Y-J (2005) J Power Sources 147:214
16. Lee SH, Koo BK, Kim J-C, Kim KM (2008) J Power Sources 184:276
17. Sato Y, Nakano T, Kobayakawa K, Kawai T, Yokoyama A (1998) J Power Sources 75:271
18. Ohzuku T, Ueda A, Nagayama M, Iwakoshi Y, Komori H (1993) Electrochim Acta 38:1159
19. Lu Z, Beaulieu LY, Donaberger RA, Thomas CL, Dahn JR (2002) J Electrochem Soc 149:A778
20. Chen Z, Dahn JR (2004) Electrochem Solid-State Lett 7:A11